

Distribution Features of Underwater Static Electric Field Intensity of Warship in Typical Restricted Sea Areas

Cong Chen, Jingxuan Yang^{*}, Chuyang Du, and Lifeng Si

Abstract—In order to study the distribution feature of the underwater electric field intensity produced by a ship in restricted seawaters, a horizontal DC electric dipole is used as the equivalent field source. Firstly, four kinds of field models are established. Secondly, the expressions of underwater electric field strength produced by a horizontal DC electric dipole in the sea areas with upright bank is derived based on the mirror theory of static electric field. Then, based on this, the distribution features of the electric field intensity and the influence of the bank on the electric field are studied by numerical simulation. The simulated results show that the main characteristics of field strength distribution in restricted seawaters are consistent with those without bank, but it makes the absolute value of electric strength increased. The field point is closer to the vertical bank, and it generally presents greater influence on the absolute value of electric strength. But the influences of single vertical and parallel banks on the three-component field strength are different. The effect of bank on field intensity distribution in other restricted seawaters can be regarded as superimposed effects of a series of vertical or parallel banks. Finally, the rectangle marine environment is simulated in laboratory, and the horizontal components of electric field intensity distribution on a certain depth plane under the simulated field source are measured. These theoretical derivation and analytical conclusions of simulation are further confirmed by comparing with the simulated results.

1. INTRODUCTION

With the development of underwater-acoustical countermeasure, vibration and noise reduction, degaussing, and other technologies, it is particularly difficult to detect the acoustic and magnetic fields of warships. It is urgent to explore new target characteristics as the signal for underwater weapon to detect and strike targets [1]. Corrosion-related electrostatic field (CRSE) as an important feature of ship target can only be reduced but not eliminated under the existing technical conditions, and can be used to control fuze action [2] and target positioning [3]. When underwater weapons and detection arrays equipped with electric field sensors are used in coastal combat environment, the effect of horizontal interface of medium and boundary of shore wall on field distribution should be fully considered so as to realize early warning, reconnaissance, guidance, and strike to optimize the design of electric field stealth of warships [4].

Some field models with shore boundary have been established in the previous studies on the distribution of underwater electric field of warships by using boundary element method [5], finite element method [6], and equivalent source method [7], and only a few have been involved in response field models with shore boundary. Since the electric dipole along the bow direction can be used as the equivalent field source for the main characteristics of the underwater electric field of a warship in the far field condition, the scalar potentials of the static horizontal dipole in the three-layer “infinite” model and special position bank (perpendicular to and parallel to the dipole) model are solved [8]. However, compared with scalar

Received 14 October 2019, Accepted 26 April 2020, Scheduled 10 June 2020

^{*} Corresponding author: Jingxuan Yang (1114884300@qq.com).

The authors are with the Department of Basic Courses, Naval University of Engineering, Wuhan 430033, China.

potential, it is more meaningful to grasp the three-component field intensity distribution characteristics for realizing and localization target by utilizing the characteristics of warship electric field [3]. In addition, the shape of upright interface in actual marine environment and the relative position of ship are different. Especially when the underwater electric field of the simulated field source is measured in the laboratory, the influence of the surrounding boundary on the field distribution is enough to be detected under the existing technical conditions, and there is a gap between the measured results of scalar potential and the simulated values under the “three-layer no-bank model” at the extreme point and near-shore field point, even though the corresponding signals can already be detected for boundary location [9]. It is necessary to establish a field model which is more similar to the experimental conditions and study the characteristics of field distribution under the corresponding boundary conditions in order to verify the correctness of the modeling results by using the measured results in limited space.

The so-called typical restricted sea areas in this paper are four kinds of common coastal marine environments: single vertical coastal wall, right angle, archipelagos, and rectangle. On the basis of previous studies, static electric dipole is still used as the equivalent field source for the main characteristics of underwater electric field of warships. Firstly, the field model of typical restricted sea area is established. Then the distribution of electric field in seawater is calculated based on image method; the distribution characteristics of electric dipole underwater electric field under different boundary conditions are further studied by numerical simulation method; finally, the corresponding simulated field source and ocean environment are designed in the laboratory, and the horizontal direction component of electric intensity in a certain depth plane is measured to verify the theoretical deduction and research conclusions.

2. THEORETICAL DEDUCTION OF THE DISTRIBUTION OF UNDERWATER ELECTROSTATIC FIELD INTENSITY OF A WARSHIP IN A TYPICAL RESTRICTED SEA AREA

In the actual marine environment, the shape of the shore bank and its relative position with the ship are quite different, but the equivalent field source of the underwater electric field of the warship can be decomposed into components perpendicular to and parallel to the shore bank when only a single bank exists. In this paper, we first derive the underwater electric intensity of a ship with a single shore bank perpendicular to or parallel to the ship’s course (hereinafter referred to as the vertical shore bank and parallel shore bank, respectively). The boundary of the shore bank in other complex marine environments can be approximated to the combination of the two sorts of shore banks. Based on this, the field models of angular, archipelagos, rectangular sea areas are established, and the electric intensity of underwater electrostatic field of warships under the corresponding marine environment is derived.

According to Archie’s formula, the resistivity of porous rock is related to water saturation and porosity [10]. When the material structures of seabed and shore bank are the same, and there is no obvious change in the conductivity of seawater in limited space, they can be simplified to the same material only by considering the conductivity characteristics. In this paper, both of them are expressed as shore bank media. Then the whole space is occupied by air, sea water, and shore bank, which are respectively expressed as V_i , conductivity, permeability, and capacitance as $(\sigma_i, \mu_i, \varepsilon_i)$, $i = 0, 1, 2$.

The coordinate system shown in Fig. 1(a) and Fig. 1(b) is established. The horizontal plane is taken as the xOy plane. The z axis is perpendicular to the water surface and points to the center of the earth. The depth of the sea water is D . In this paper, the main characteristics of the underwater electric field can be simulated by the electric dipole along the x direction the same as the ship’s course, i.e., $Id\mathbf{l} = I_x d\mathbf{l}\mathbf{i}$, whose position is $(x_0, y_0, z_0) \in V_1$.

2.1. Underwater Electrostatic Field of Warship with a Single Upright Bank

2.1.1. Underwater Electrostatic Field of Ships with Vertical Bank

According to the uniqueness principle, it is proved that the field intensity at a point in seawater is the superposition of a series of upright distributed dipoles (hereinafter referred to as source dipoles group, numbered (0) obtained from the field source and its mirror image of two horizontal layered interfaces

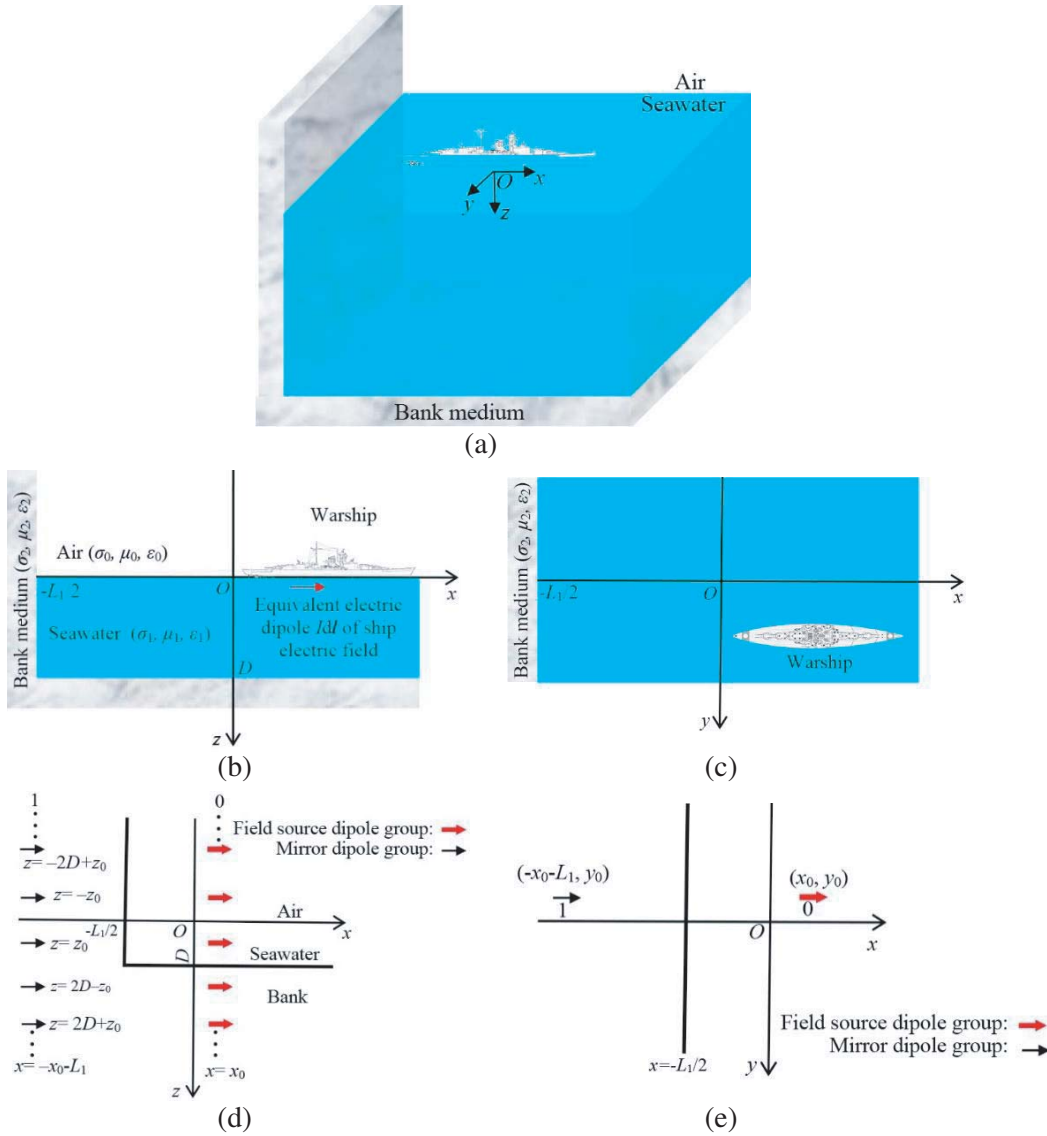


Figure 1. Three-layer vertical bank model. (a) 3-D image. (b) Main view. (c) Top view. (d) Main view of dipole groups. (e) Top view of dipole groups.

under a three-layer no-bank model. As shown in Fig. 1, the electric intensity at seawaters in the three-layer vertical bank model should be equal to the superposition of the electric field stimulated by the source dipole group and its mirror dipole group 1 on the seawater-coastal bank boundary. The scalar potential at the seawaters field point (x, y, z) can be obtained:

$$\Phi(x, y, z) = \Phi_0(x, y, z) + \Phi_1(x, y, z) \tag{1}$$

Correspondingly, the electric field intensity at the field point (x, y, z) is:

$$\begin{aligned} E(x, y, z) &= -\nabla \cdot \Phi(x, y, z) = -\frac{\partial(\Phi_0 + \Phi_1)}{\partial x} \mathbf{i} - \frac{\partial(\Phi_0 + \Phi_1)}{\partial y} \mathbf{j} - \frac{\partial(\Phi_0 + \Phi_1)}{\partial z} \mathbf{k} \\ &= (E_{x0} + E_{x1})\mathbf{i} + (E_{y0} + E_{y1})\mathbf{j} + (E_{z0} + E_{z1})\mathbf{k} \end{aligned} \tag{2}$$

E_{x0} , E_{y0} , and E_{z0} can be calculated from [8]. Furthermore E_{x0} , E_{y0} , and E_{z0} can be calculated from Φ_1 as follows:

$$E_{x1}(x, y, z) = - \sum_{k=1}^{\infty} \left[-\eta^{k+1} I_x dl \frac{\mathbf{r}_{k11}^2 - 3(\mathbf{r}_{k11} \cdot \mathbf{i})^2}{4\pi\sigma_1 r_{k11}^5} - \eta^{k+1} I_x dl \frac{\mathbf{r}_{k21}^2 - 3(\mathbf{r}_{k21} \cdot \mathbf{i})^2}{4\pi\sigma_1 r_{k21}^5} \right] - \sum_{m=0}^{\infty} \left[-\eta^{m+1} I_x dl \frac{\mathbf{r}_{m11}^2 - 3(\mathbf{r}_{m11} \cdot \mathbf{i})^2}{4\pi\sigma_1 4\pi\sigma_1 r_{m11}^5} - \eta^{m+1} I_x dl \frac{\mathbf{r}_{m21}^2 - 3(\mathbf{r}_{m21} \cdot \mathbf{i})^2}{4\pi\sigma_1 r_{m21}^5} \right] \quad (3)$$

$$E_{y1}(x, y, z) = - \sum_{k=1}^{\infty} \left[-\eta^{k+1} I_x dl \frac{(\mathbf{r}_{k11} \cdot \mathbf{j})(\mathbf{r}_{k11} \cdot \mathbf{i})}{4\pi\sigma_1 r_{k11}^5} - \eta^{k+1} I_x dl \frac{(\mathbf{r}_{k21} \cdot \mathbf{j})(\mathbf{r}_{k21} \cdot \mathbf{i})}{4\pi\sigma_1 r_{k21}^5} \right] - \sum_{m=0}^{\infty} \left[-\eta^{m+1} I_x dl \frac{(\mathbf{r}_{m11} \cdot \mathbf{j})(\mathbf{r}_{m11} \cdot \mathbf{i})}{4\pi\sigma_1 r_{m11}^5} - \eta^{m+1} I_x dl \frac{(\mathbf{r}_{m21} \cdot \mathbf{j})(\mathbf{r}_{m21} \cdot \mathbf{i})}{4\pi\sigma_1 r_{m21}^5} \right] \quad (4)$$

$$E_{z1}(x, y, z) = - \sum_{k=1}^{\infty} \left[-\eta^{k+1} I_x dl \frac{(\mathbf{r}_{k11} \cdot \mathbf{k})(\mathbf{r}_{k11} \cdot \mathbf{i})}{4\pi\sigma_1 r_{k11}^5} - \eta^{k+1} I_x dl \frac{(\mathbf{r}_{k21} \cdot \mathbf{k})(\mathbf{r}_{k21} \cdot \mathbf{i})}{4\pi\sigma_1 r_{k21}^5} \right] - \sum_{m=0}^{\infty} \left[-\eta^{m+1} I_x dl \frac{(\mathbf{r}_{m11} \cdot \mathbf{k})(\mathbf{r}_{m11} \cdot \mathbf{i})}{4\pi\sigma_1 r_{m11}^5} - \eta^{m+1} I_x dl \frac{(\mathbf{r}_{m21} \cdot \mathbf{k})(\mathbf{r}_{m21} \cdot \mathbf{i})}{4\pi\sigma_1 r_{m21}^5} \right] \quad (5)$$

$$\eta = \frac{\sigma_1 - \sigma_2}{\sigma_1 + \sigma_2}, \quad k = 0, 1, 2, \dots, m = 0, 1, 2, \dots \quad (6)$$

The electric dipole moment of mirror dipole is $\eta^{k+1} I_x d\mathbf{l}$ or $-\eta^{m+1} I_x d\mathbf{l}$; \mathbf{r}_{k11} , \mathbf{r}_{k21} , \mathbf{r}_{m11} , and \mathbf{r}_{m21} are position vectors from field point to mirror dipole; and the position of mirror dipoles on the xOy plane is $(-x_0 - L_1, y_0)$, then,

$$\begin{cases} \mathbf{r}_{k11} = (x + x_0 + L_1)\mathbf{i} + (y - y_0)\mathbf{j} + (z - 2kD + z_0)\mathbf{k} \\ \mathbf{r}_{k21} = (x + x_0 + L_1)\mathbf{i} + (y - y_0)\mathbf{j} + (z - 2kD - z_0)\mathbf{k} \\ \mathbf{r}_{m11} = (x + x_0 + L_1)\mathbf{i} + (y - y_0)\mathbf{j} + (z + 2mD - z_0)\mathbf{k} \\ \mathbf{r}_{m21} = (x + x_0 + L_1)\mathbf{i} + (y - y_0)\mathbf{j} + (z + 2mD + z_0)\mathbf{k} \end{cases} \quad (7)$$

2.1.2. Underwater Electrostatic Field of Ships with Parallel Bank

As shown in Fig. 2, the calculation method of the underwater electric field of a warship in the parallel bank model is the same as that in the vertical one. In the three-layer parallel bank model (where the bank boundary is projected on the $y = -L_2/2$ plane), the electric field intensity at the field point (x, y, z) in the sea water is the superposition of the field source dipole group and the mirror dipole group 4 at the point, respectively.

$$E(x, y, z) = (E_{x0} + E_{x4})\mathbf{i} + (E_{y0} + E_{y4})\mathbf{j} + (E_{z0} + E_{z4})\mathbf{k} \quad (8)$$

The electric dipole moment of mirror dipole is $\eta^{k+1} I_x d\mathbf{l}$ or $\eta^{m+1} I_x d\mathbf{l}$, and the position vectors from field point to mirror dipole are respectively,

$$\begin{cases} \mathbf{r}_{k14} = (x - x_0)\mathbf{i} + (y + y_0 - L_2)\mathbf{j} + (z - 2kD + z_0)\mathbf{k} \\ \mathbf{r}_{k24} = (x - x_0)\mathbf{i} + (y + y_0 - L_2)\mathbf{j} + (z - 2kD - z_0)\mathbf{k} \\ \mathbf{r}_{m14} = (x - x_0)\mathbf{i} + (y + y_0 - L_2)\mathbf{j} + (z + 2mD - z_0)\mathbf{k} \\ \mathbf{r}_{m24} = (x - x_0)\mathbf{i} + (y + y_0 - L_2)\mathbf{j} + (z + 2mD + z_0)\mathbf{k} \end{cases} \quad (9)$$

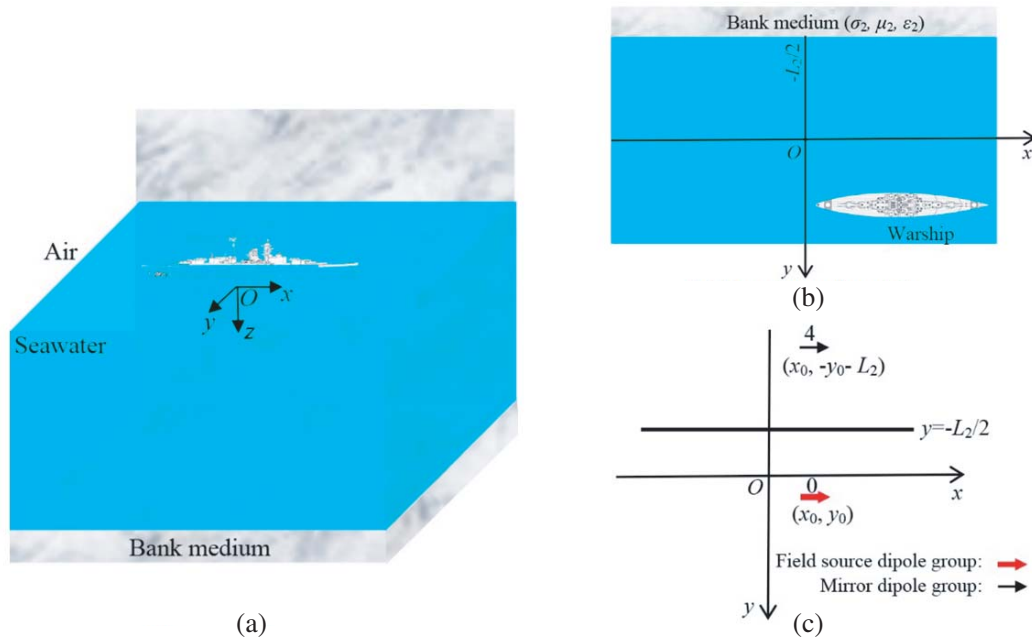


Figure 2. Three-layer parallel bank model. (a) 3-D image. (b) Top view of model. (c) Top view of dipole groups.

2.2. Underwater Electrostatic Field of Ships in Three-Layer Right-Angled Sea Area

As shown in Fig. 3(a), assuming that the projections on the xOy plane satisfy the equations respectively: $x = -L_1/2$ and $y = -L_2/2$, the three-layer right-angled sea area studied in this paper is a three-layer horizontal stratified sea environment with vertical and parallel shore banks which are perpendicular to and parallel to the ship’s course. As shown in Fig. 3(b), the field intensity at the field point (x, y, z) in seawater is the superposition of the field source dipole group and the three mirror dipole groups at the

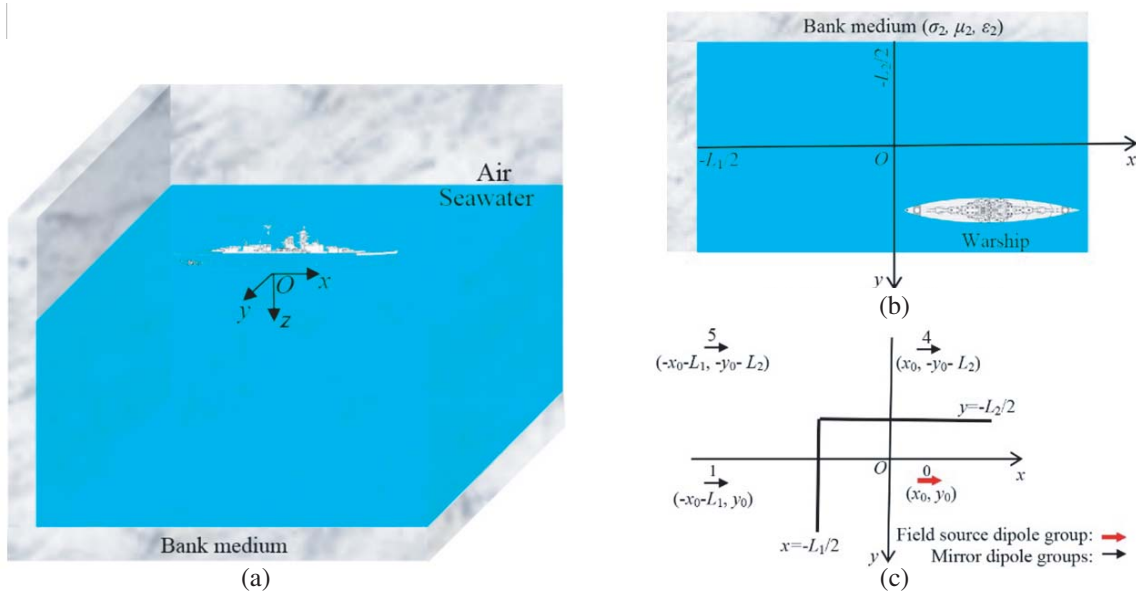


Figure 3. Three-layer right-angled sea area model. (a) Top view of model. (b) Top view of model. (c) Top view of dipole groups.

same point.

$$E(x, y, z) = (E_{x0} + E_{x1} + E_{x4} + E_{x5})\mathbf{i} + (E_{y0} + E_{y1} + E_{y4} + E_{y5})\mathbf{j} + (E_{z0} + E_{z1} + E_{z4} + E_{z5})\mathbf{k} \quad (10)$$

As shown in Fig. 3(b), the projection positions and electric dipole moments of the first and fourth groups of mirror dipoles on the xOy plane are the same as those with only vertical and parallel banks, and the electric dipole moments of the fifth group of mirror dipoles are $-\eta^{k+2}I_x d\mathbf{l}$ or $-\eta^{m+2}I_x d\mathbf{l}$, and their projection positions on the xOy plane are $(-x_0 - L_1, -y_0 - L_2)$.

2.3. Underwater Electrostatic Field of Ships in Three-Layer Archipelagos Area

As shown in Fig. 4(a), the three-layer archipelagos sea area studied in this paper is based on the parallel bank wall model mentioned above, and there are two parallel bank boundaries in the horizontal direction ($y = -L_2/2$ and $y = L_2/2$ respectively on the xOy plane). When the mirror method is used to solve the distribution of electrostatic field in seawater, the field source dipole group will generate infinite sets of mirror dipole groups on the boundary of both sides of the sea. According to the influence of the number of mirrors on the effective correction coefficient, as shown in Fig. 4(b), for simplification, it is better to consider only the result of one mirror image in the field space described in this paper, i.e., the electric dipole moments of the third and fourth groups of mirror dipole are $\eta^{k+2}I_x d\mathbf{l}$ or $\eta^{m+2}I_x d\mathbf{l}$, and their projection positions on the xOy plane are $(x_0, -y_0 + L_2)$, $(x_0, -y_0 - L_2)$, respectively. The electric field intensity at the point (x, y, z) of seawaters is as follows:

$$E(x, y, z) = (E_{x0} + E_{x3} + E_{x4})\mathbf{i} + (E_{y0} + E_{y3} + E_{y4})\mathbf{j} + (E_{z0} + E_{z3} + E_{z4})\mathbf{k} \quad (11)$$

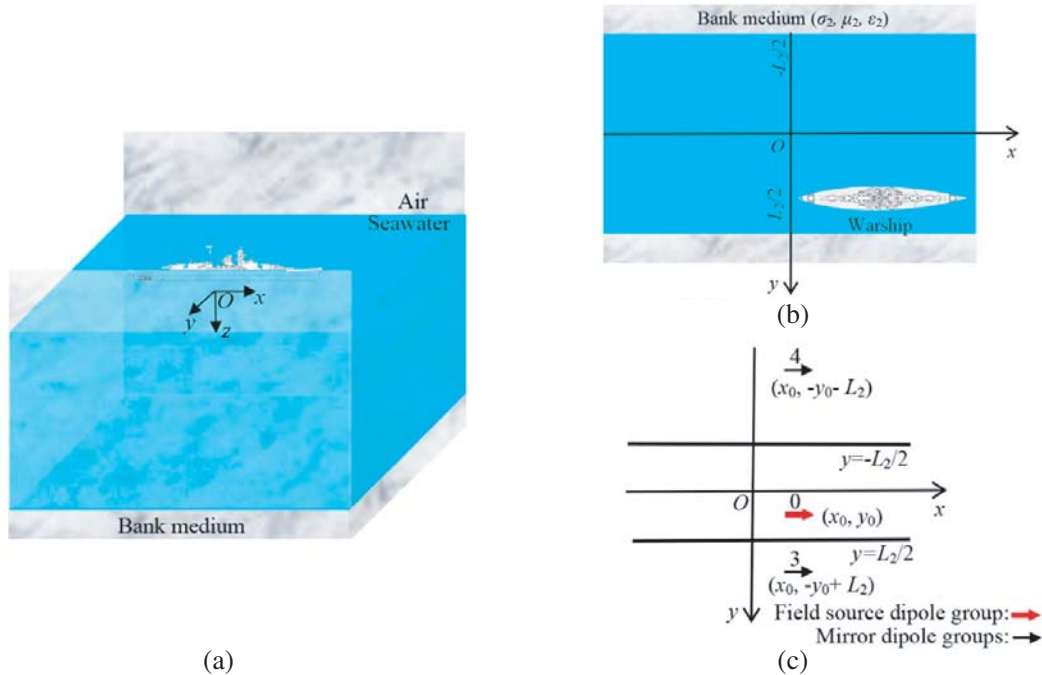


Figure 4. Three-layer archipelagos sea area model. (a) 3-D image. (b) Top view of model. (c) Top view of dipole groups.

2.4. Underwater Electrostatic Field of Ships in Rectangular Sea Area

As shown in Fig. 5(a), the rectangular sea area studied in this paper is a three-layer horizontal stratification with upright shore banks around it. It is assumed that the boundary of the shore bank is projected into rectangles with side lengths of $L_1 \times L_2$ on the xOy plane, and O is the origin of the

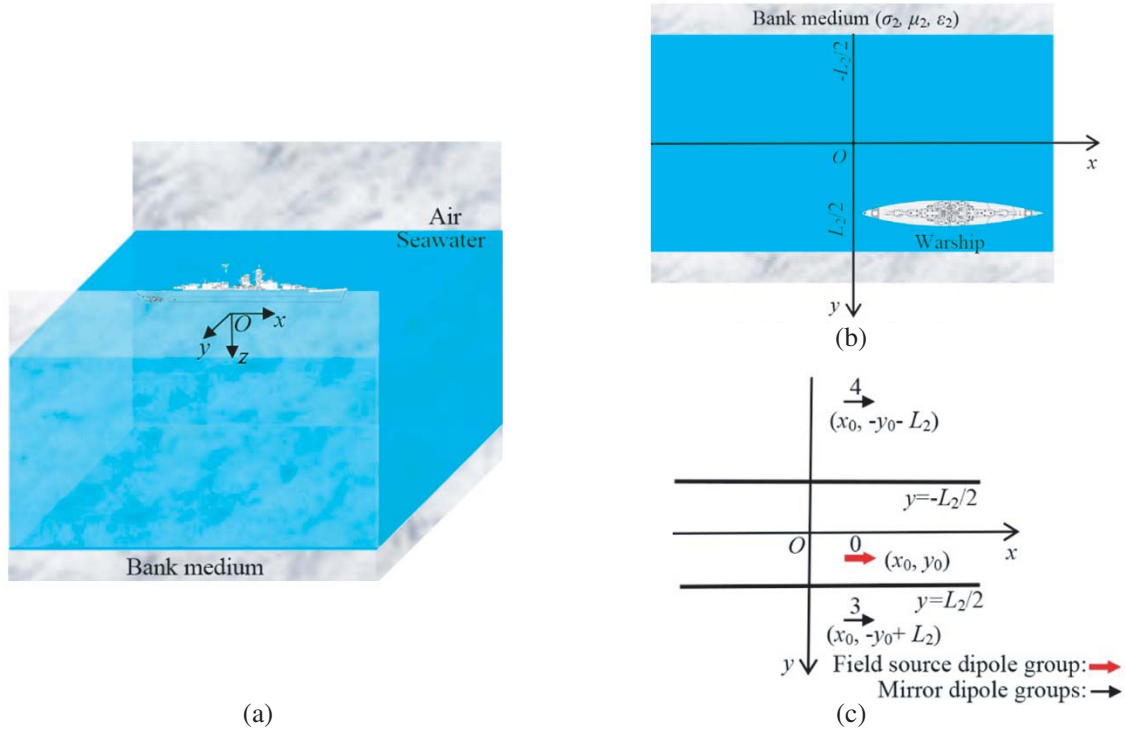


Figure 5. Three-layer rectangular sea area model. (a) 3-D image. (b) Top view of model. (c) Top view of dipole groups.

coordinate plane located at the geometric center of the rectangle. Using the mirror method, eight sets of mirror dipoles will be generated by the source dipole group through four seawater-bank interfaces, and their positions and electrical dipole moments are shown in Table 1.

Table 1. Projection position and electrical dipole moment of mirror dipoles on xOy plane.

Mirror or field source dipole groups	Position	Dipole moment	Mirror dipole groups	Position	Dipole moment
No. 0	(x_0, y_0)	$\eta^k I_x d\mathbf{l}$ or $\eta^m I_x d\mathbf{l}$	No. 1	$(-x_0 - L_1, y_0)$	$-\eta^{k+1} I_x d\mathbf{l}$ or $-\eta^{m+1} I_x d\mathbf{l}$
			No. 2	$(-x_0 + L_1, y_0)$	$-\eta^{k+1} I_x d\mathbf{l}$ or $-\eta^{m+1} I_x d\mathbf{l}$
No. 3	$(x_0, -y_0 + L_2)$	$\eta^{k+1} I_x d\mathbf{l}$ or $\eta^{m+1} I_x d\mathbf{l}$	No. 5	$(-x_0 - L_1, -y_0 - L_2)$	$-\eta^{k+2} I_x d\mathbf{l}$ or $-\eta^{m+2} I_x d\mathbf{l}$
			No. 6	$(-x_0 + L_1, -y_0 - L_2)$	$-\eta^{k+2} I_x d\mathbf{l}$ or $-\eta^{m+2} I_x d\mathbf{l}$
No. 4	$(x_0, -y_0 - L_2)$	$\eta^{k+1} I_x d\mathbf{l}$ or $\eta^{m+1} I_x d\mathbf{l}$	No. 7	$(-x_0 - L_1, -y_0 + L_2)$	$-\eta^{k+2} I_x d\mathbf{l}$ or $-\eta^{m+2} I_x d\mathbf{l}$
			No. 8	$(-x_0 + L_1, -y_0 + L_2)$	$-\eta^{k+2} I_x d\mathbf{l}$ or $-\eta^{m+2} I_x d\mathbf{l}$

Note: The z coordinates of each mirror dipole group (source dipole group) are the following four groups:
 $z_{k1i} = 2kD + z_0$, $z_{k2i} = 2kD - z_0$, $z_{m1i} = -2mD - z_0$, $z_{m2i} = 2mD + z_0$.

The value of i is only determined by the numbering order of the mirror dipole projection position on the xOy plane in Fig. 2. The electric field intensity produced by source dipole group ($i = 0$) or the

mirror dipole groups ($i = 1, 2, 3 \dots 8$) alone at the field point (x, y, z) is as follows:

$$E_{xi}(x, y, z) = - \sum_{k=1}^{\infty} \left[(-1)^p \eta^{k+q} I_x dl \frac{r_{k1i}^2 - 3(r_{k1i} \cdot i)^2}{4\pi\sigma_1 r_{k1i}^5} + (-1)^p \eta^{k+q} I_x dl \frac{r_{k2i}^2 - 3(r_{k2i} \cdot i)^2}{4\pi\sigma_1 r_{k2i}^5} \right] - \sum_{m=0}^{\infty} \left[(-1)^p \eta^{m+q} I_x dl \frac{r_{m1i}^2 - 3(r_{m1i} \cdot i)^2}{4\pi\sigma_1 4\pi\sigma_1 r_{m1i}^5} + (-1)^p \eta^{m+q} I_x dl \frac{r_{m2i}^2 - 3(r_{m2i} \cdot i)^2}{4\pi\sigma_1 r_{m2i}^5} \right] \quad (12)$$

$$E_{yi}(x, y, z) = - \sum_{k=1}^{\infty} \left[(-1)^p \eta^{k+q} I_x dl \frac{(r_{k1i} \cdot j)(r_{k1i} \cdot i)}{4\pi\sigma_1 r_{k1i}^5} + (-1)^p \eta^{k+q} I_x dl \frac{(r_{k2i} \cdot j)(r_{k2i} \cdot i)}{4\pi\sigma_1 r_{k2i}^5} \right] - \sum_{m=0}^{\infty} \left[(-1)^p \eta^{m+q} I_x dl \frac{(r_{m1i} \cdot j)(r_{m1i} \cdot i)}{4\pi\sigma_1 r_{m1i}^5} + (-1)^p \eta^{m+q} I_x dl \frac{(r_{m2i} \cdot j)(r_{m2i} \cdot i)}{4\pi\sigma_1 r_{m2i}^5} \right] \quad (13)$$

$$E_{zi}(x, y, z) = - \sum_{k=1}^{\infty} \left[(-1)^p \eta^{k+1} I_x dl \frac{(r_{k1i} \cdot k)(r_{k1i} \cdot i)}{4\pi\sigma_1 r_{k1i}^5} + (-1)^p \eta^{k+1} I_x dl \frac{(r_{k2i} \cdot k)(r_{k2i} \cdot i)}{4\pi\sigma_1 r_{k2i}^5} \right] - \sum_{m=0}^{\infty} \left[(-1)^p \eta^{m+1} I_x dl \frac{(r_{m1i} \cdot k)(r_{m1i} \cdot i)}{4\pi\sigma_1 r_{m1i}^5} + (-1)^p \eta^{m+1} I_x dl \frac{(r_{m2i} \cdot k)(r_{m2i} \cdot i)}{4\pi\sigma_1 r_{m2i}^5} \right] \quad (14)$$

$$p = \begin{cases} 1 & (i = 0, 3, 4) \\ -1 & (i = 1, 2, 5, 6, 7, 8) \end{cases} \quad q = \begin{cases} 0 & (i = 0) \\ 1 & (i = 1, 2, 3, 4) \\ 2 & (i = 5, 6, 7, 8) \end{cases} \quad (15)$$

\mathbf{r}_{k1i} , \mathbf{r}_{k2i} , \mathbf{r}_{m1i} , and \mathbf{r}_{m2i} are position vectors from field point to mirror dipole, respectively, which can be calculated by Equations (7) and (9). In the rectangular sea area model, electric field intensity at any field point $(x, y, z) \in V_1$ can be expressed as follows:

$$E(x, y, z) = \sum_{i=0}^8 E_{xi} \mathbf{i} + \sum_{i=0}^8 E_{yi} \mathbf{j} + \sum_{i=0}^8 E_{zi} \mathbf{k} \quad (16)$$

3. SIMULATION ANALYSIS OF THE DISTRIBUTION CHARACTERISTICS OF WARSHIPS' UNDERWATER ELECTROSTATIC FIELD IN HORIZONTAL STRATIFIED SEA AREA

In order to study the distribution characteristics of the underwater electrostatic field, the electric dipole along the x direction is used as the equivalent source of the main characteristics of the electric field of the warship. Based on the theoretical derivation of the distribution of the electric intensity in the sea water mentioned above, the numerical simulation is carried out by using Equations (1)–(16). Electrical dipole moment $I_x dl = 10 \text{ A}\cdot\text{m}$, field source position $(x_0, y_0, z_0) = (0.0, 0.0, 10.0) \text{ m}$, sea water depth $D = 50.0 \text{ m}$, sea water conductivity $\sigma_1 = 4.0 \text{ S/m}$, and shore bank conductivity $\sigma_2 = 0.4 \text{ S/m}$.

3.1. Simulation Analysis of Ships' Underwater Electrostatic Field in Three-Layer Sea Area with a Single Upright Bank

3.1.1. Simulation Analysis of Ships' Underwater Electrostatic Field in Three-Layer Sea Area with a Single Vertical Bank

Assuming $L_1 = 80.0 \text{ m}$, firstly, the E distribution on $z = 20.0 \text{ m}$ plane is calculated according to Equations (3)–(7). The simulated vector field map of the field intensity distribution at different field points on the depth plane is shown in Fig. 6(a). E_x , E_y , and E_z on the field lines paralleled to yOz plane with equal interval distribution along x direction are calculated respectively under two kinds of

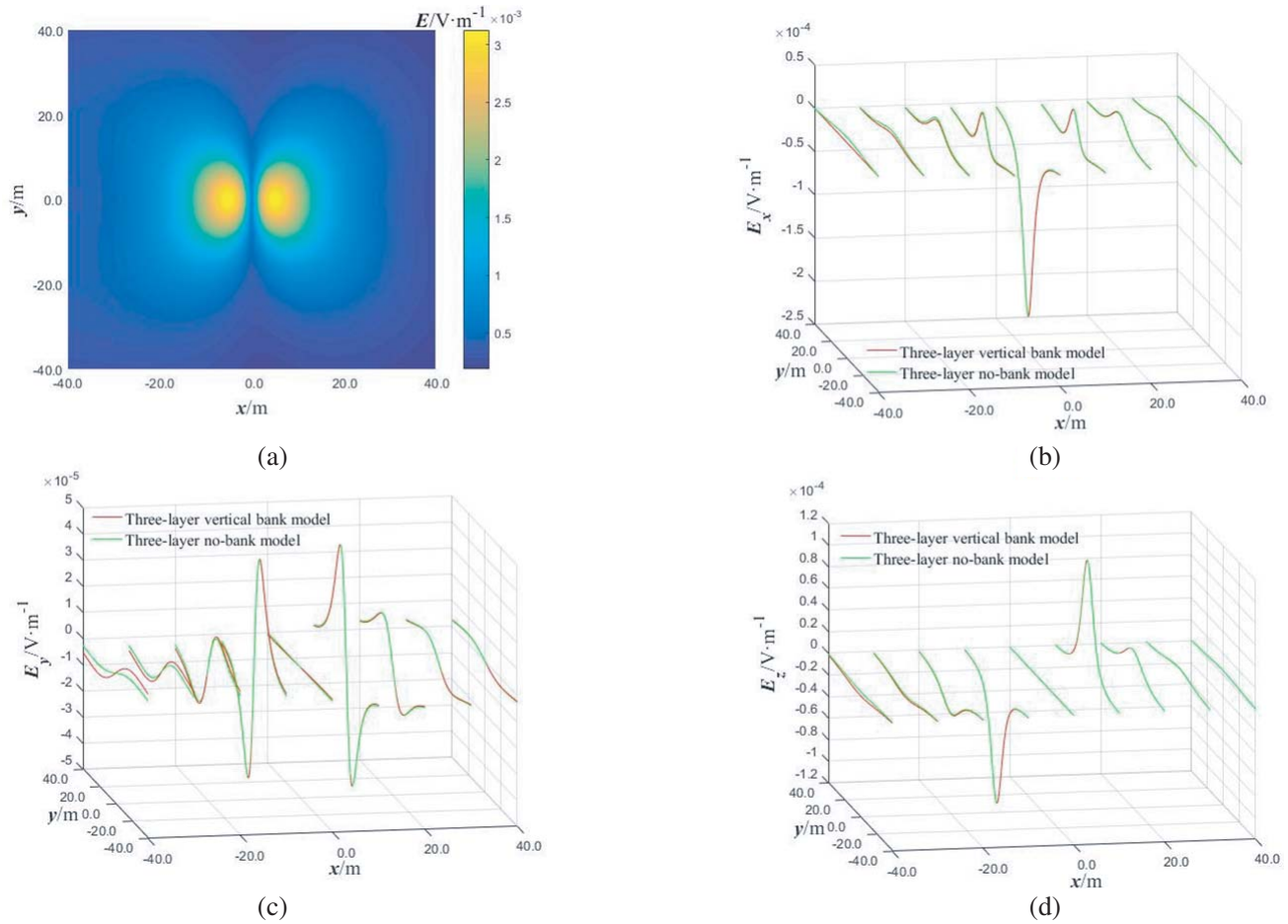


Figure 6. E distribution at $z = 20.0$ m with vertical bank existing. (a) Top view of E . (b) E_x . (c) E_y . (d) E_z .

conditions: the vertical shore bank and no shore bank. The simulation results are shown in Figs. 6(c), (d), and (e), respectively.

Figure 6 shows that,

(1) The distribution trend of the underwater static electric field of a warship in a horizontal stratified marine environment with vertical bank is consistent with that without [8]. The main futures of the electric field still have obvious characteristics of passage.

(2) The vertical bank increases the field intensity modulus at sites near the bank, and the vertical distance between the site and the bank is closer. The increase of the field intensity modulus is more obvious, that is to say, the bank makes greater influence on the increase of the field intensity modulus.

(3) The influence of the bank on the distribution of the three-component electric field intensity in the tangential direction of the shore bank is different. It increases $|E_y|$ at all the field points except the mid-longitudinal section ($y = 0.0$ m), and the trend of influence increases first and then decreases with the increase of the vertical distance between the field points and the mid-longitudinal section. For $|E_x|$ and $|E_z|$, the closer the site is to the midship longitudinal section, the more significant the effect is.

The fundamental reason for the above phenomenon is that the bank is a high resistance body relative to the sea water, which will hinder the current flow, thus increasing the scalar potential of the site near the bank wall and increasing the field intensity modulus; moreover, the greater the vertical distance is from the bank wall, the more significant the impact is. Starting from the field intensity expressions (3)–(7) excited at the field point in the sea water of mirror dipole group, it is also easy to understand that the bank has different effects on the three-component field intensity in the tangential direction of the shore wall.

3.1.2. Simulation Analysis of Ships' Underwater Electrostatic Field in Three-Layer Sea Area with a Single Parallel Bank

Assuming $L_2 = 80.0$ m, the E distribution on $z = 20.0$ m plane is calculated according to Equations (8)–(9), and E_x , E_y , and E_z on a series of field lines paralleled to xOz are distributed at equal intervals along the y direction in the depth plane with and without parallel bank. The simulation results are shown in Fig. 7.

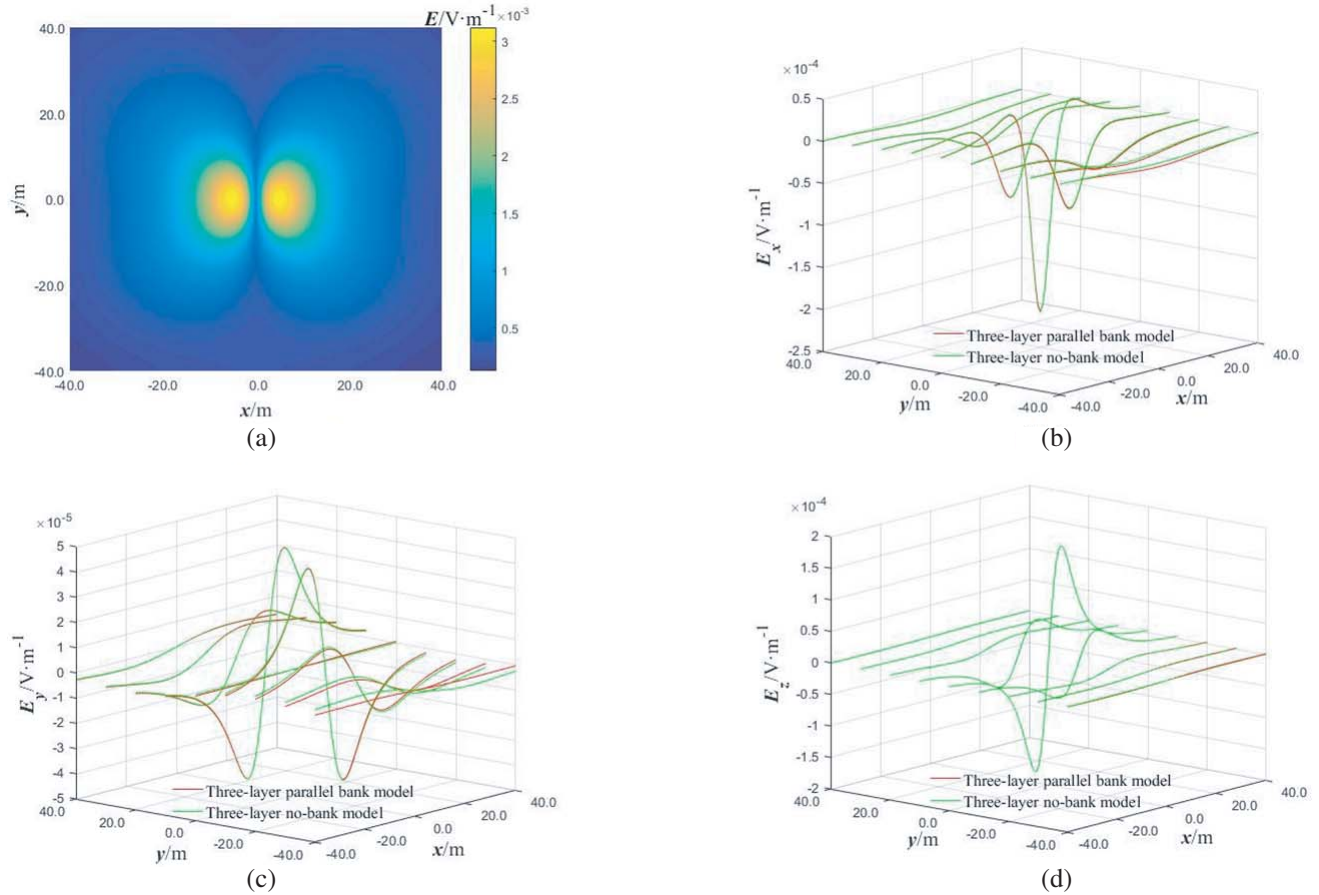


Figure 7. \mathbf{E} distribution at $z = 20.0$ m with parallel bank existing. (a) Top view of \mathbf{E} . (b) E_x . (c) E_y . (d) E_z .

As can be seen from Fig. 7,

(1) The distribution trend of the underwater electrostatic field of the warship in the horizontal stratified marine environment with vertical bank is the same as that without seacoast [9].

(2) In the normal direction of the bank, the influence of the parallel bank on the three-component field intensity is consistent with that of the vertical bank.

(3) In the tangential direction of the bank, the influence of parallel bank on the three-component field intensity is different. The boundary makes $|E_y|$, $|E_z|$ increase at all the field points except the midship cross section ($x = 0.0$ m), and the influence of the bank increases first and then decreases with the increase of the vertical distance between the field points with the midship cross section. The closer the site is to the section, the greater the influence is.

The reasons are as follows: compared with the vertical bank wall, according to the position vector expression (9) from the field point to the mirror dipole in the presence of parallel bank wall, we can understand the principles of the influence of the bank on the three-component field intensity in the tangent direction of the bank.

3.2. Simulation Analysis of Warships' Underwater Electrostatic Field in Three-Layer Right-Angle Sea Area

Taking $L_1 = 80.0$ m and $L_2 = 80.0$ m, the distribution of electrostatic field on $z = 20.0$ m plane and E_x , E_y , and E_z on the depth plane of field lines parallel to yOz with equal interval along x direction of three layers right angle sea area and three layers infinite sea area series are calculated according to Equation (10). The simulation results are shown in Fig. 8.

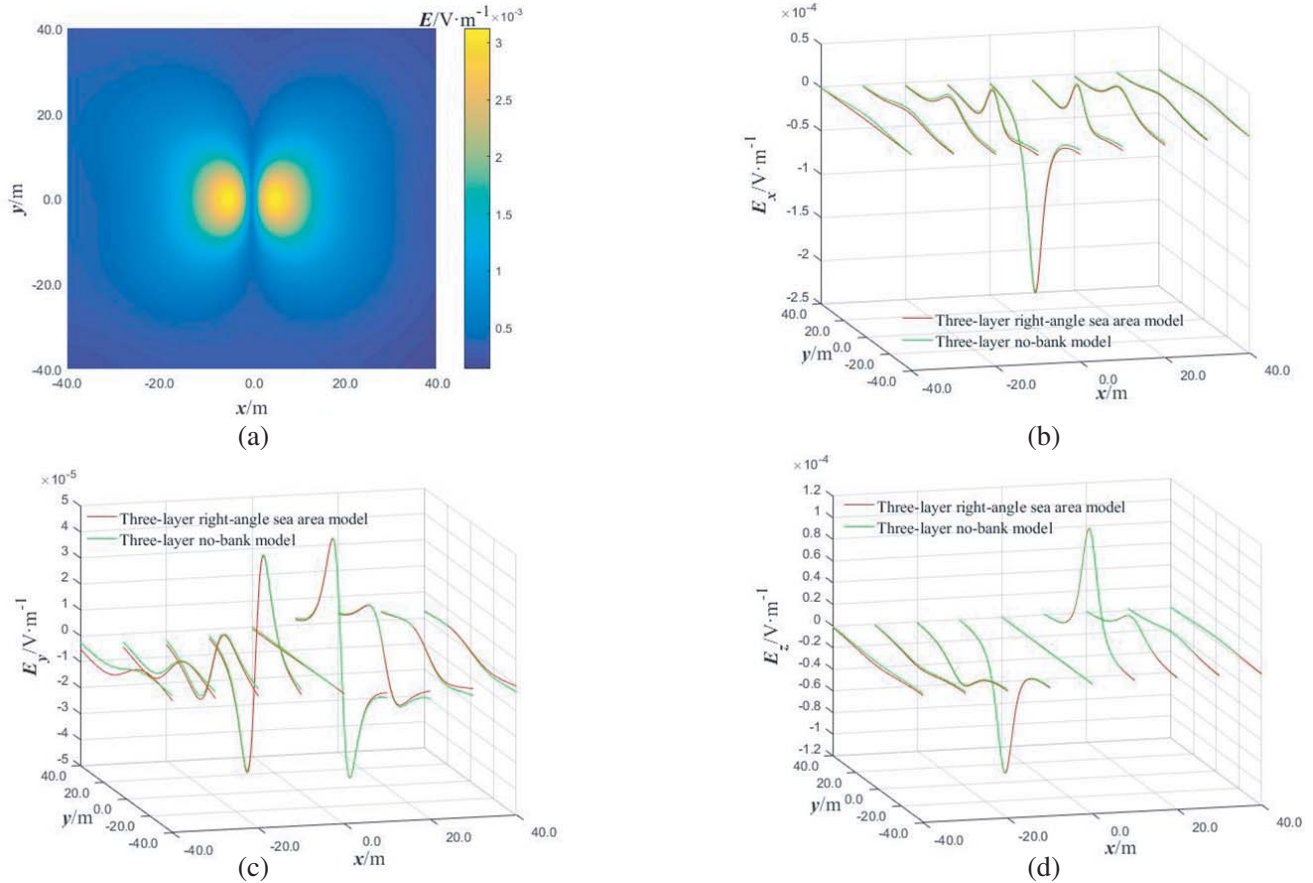


Figure 8. \mathbf{E} distribution at $z = 20.0$ m in three-layer right-angle sea area. (a) Top view of \mathbf{E} . (b) E_x . (c) E_y . (d) E_z .

It is shown in Fig. 8 that,

(1) In the three-layer right-angled sea area, the main characteristics of underwater electrostatic field distribution are not changed by the boundary of the bank [8].

(2) Under the above simulation parameters, the law of the influence of the bank boundary on the three-component field intensity is similar to that of the only vertical shore bank. That is to say, when the vertical distance between the warship and the bank is the same, the influence of the vertical bank on the distribution of the underwater electrostatic field of the warship is greater than that of the parallel shore bank.

The reason is that the main direction of current generated by the electric dipole in seawater is consistent with the electric dipole moment, so it is easy to understand that the vertical bank has more influence on the distribution of the field in seawater than the parallel bank.

3.3. Simulation Analysis of Warships' Underwater Electrostatic Field in Three-Layer Archipelagos Area

Taking $L_1 = 80.0$ m and $L_2 = 80.0$ m, the distribution of electrostatic field on $z = 20.0$ m plane is calculated according to Equation (11), and E_x , E_y , and E_z on the depth plane with equal spacing along x direction and paralleled to yOz series field lines are calculated in the sea area of waterway and without coastal bank. The simulation results are shown in Fig. 9.

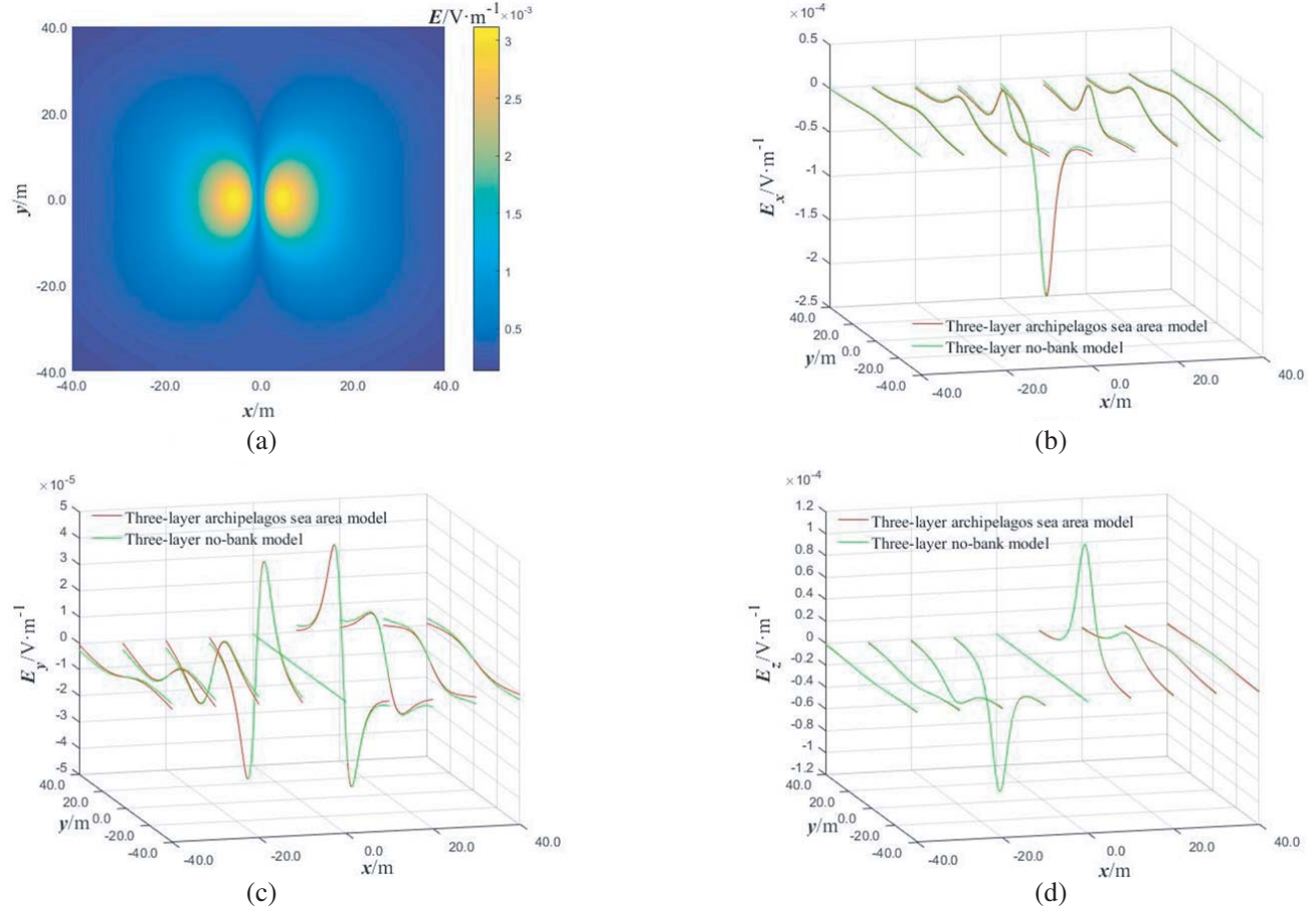


Figure 9. \mathbf{E} distribution at $z = 20.0$ m in three-layer archipelagos sea area. (a) Top view of \mathbf{E} . (b) E_x . (c) E_y . (d) E_z .

As can be seen from Fig. 9,

(1) The main characteristics of the underwater electrostatic field of a ship in the three-layer archipelagos area are consistent with those without bank.

(2) The larger the vertical distance is between the site and the mid-longitudinal section of the ship, the more obvious the effect of the shore wall is on the three-component field intensity.

3.4. Simulation Analysis of Ships' Underwater Electrostatic Field in Three-Layer Rectangular Sea Area

Taking $L_1 = 100.0$ m and $L_2 = 60.0$ m, according to Equations (12)–(16), the distribution of electrostatic field on $z = 20.0$ m plane and E_x , E_y and E_z on the series of field lines paralleled to yOz in the three-layer rectangular sea area and three-layer infinite sea area are calculated. The simulation results are shown in Fig. 10.

As can be seen from Fig. 10,

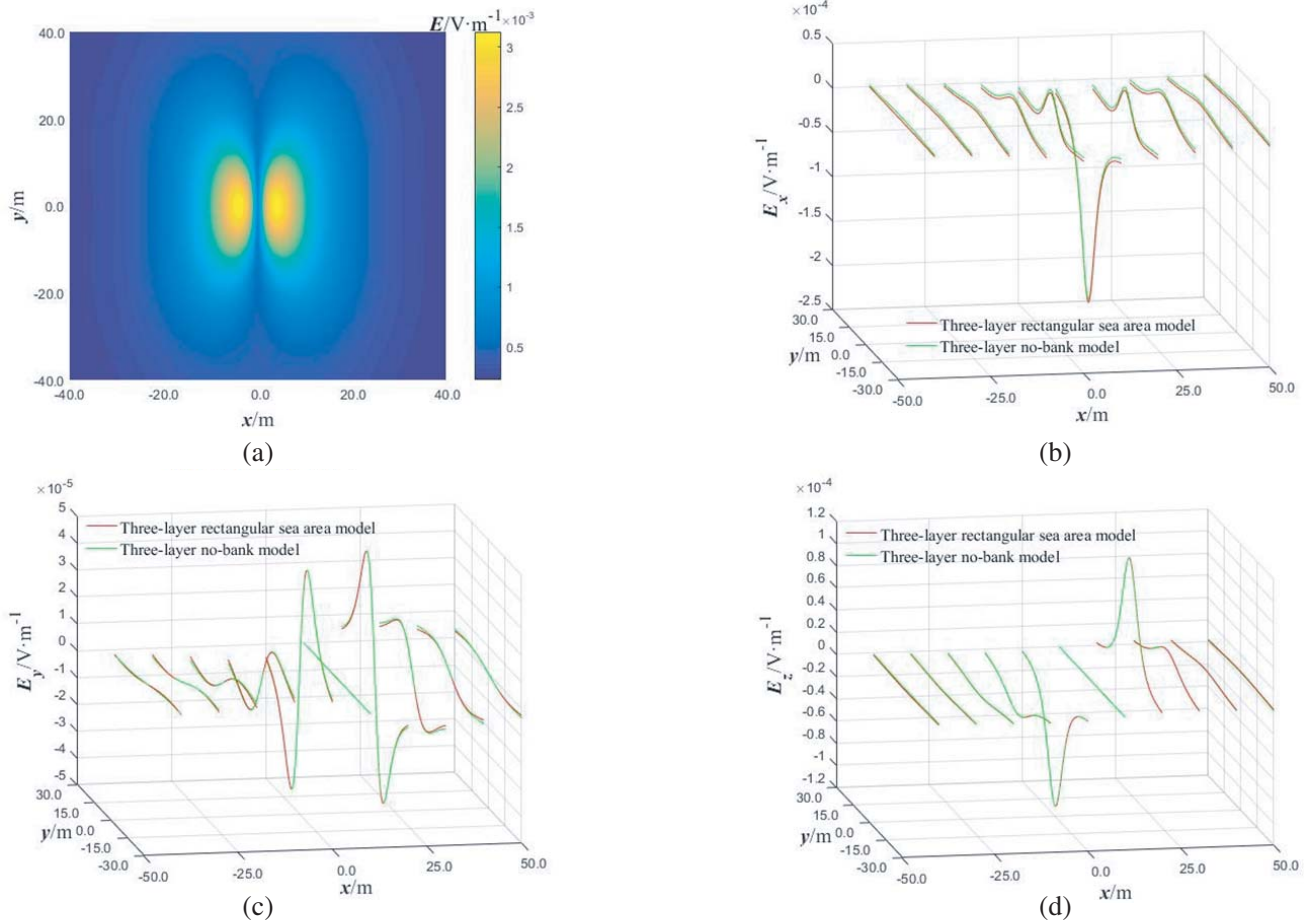


Figure 10. \mathbf{E} distribution at $z = 20.0$ m in three-layer rectangular sea area. (a) Top view of \mathbf{E} . (b) E_x . (c) E_y . (d) E_z .

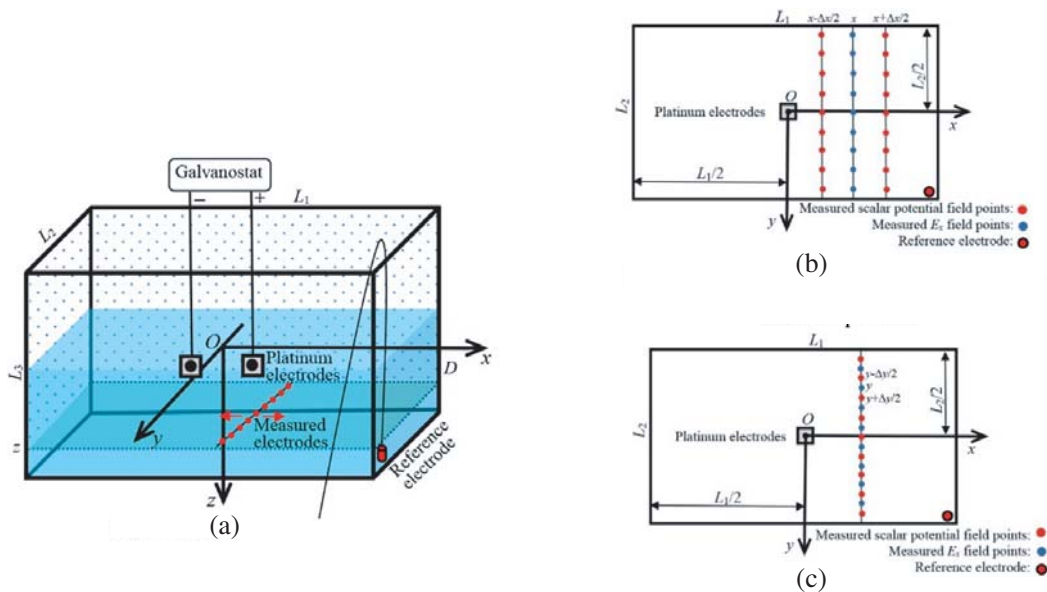


Figure 11. Experimental setup diagram. (a) 3-D image. (b) Top View of measured field point of E_x and electrode position. (c) Top View of measured field point of E_y and electrode position.

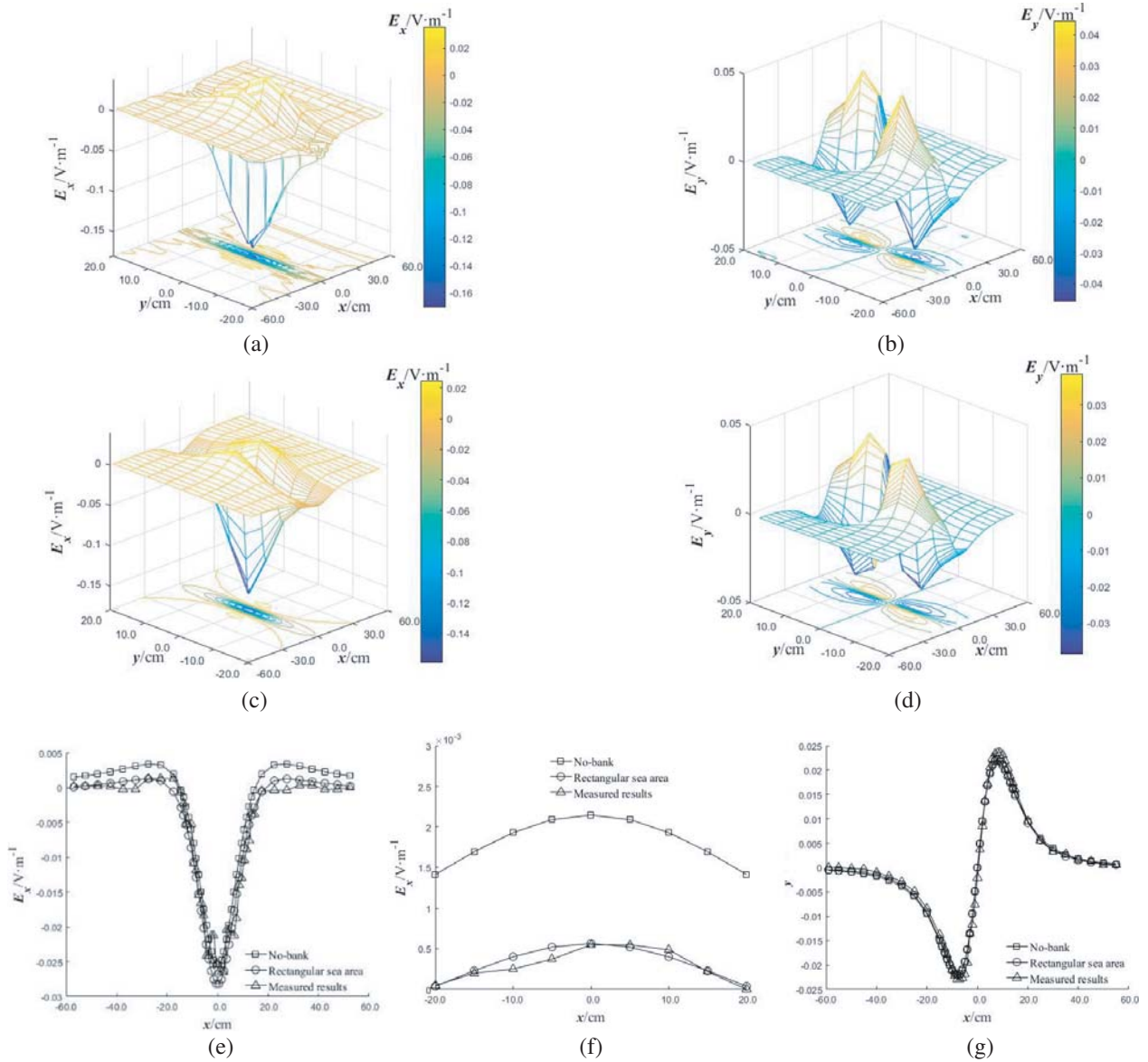


Figure 12. Results of experimental verification. (a) E_x of the measured value. (b) E_y of the measured value. (c) E_x of the simulation value. (d) E_y of the simulation value. (e) E_x on $y = 15.0$ cm. (f) E_y on $x = 52.5$ cm. (g) E_y on $y = 15.0$ cm

(1) The main characteristics of underwater electrostatic field distribution in three-layer rectangular sea area are consistent with that in infinite three-layer horizontal stratified sea area.

(2) In the three-layer rectangular sea area, the field points are closer to the mid-cross section of the ship and the two parallel shore walls. The influence of the boundary on E_x is greater, and as for E_y , the influence of the two parallel shore walls is particularly obvious. The influence of the two vertical shore walls on E_z is more prominent.

4. EXPERIMENTAL VERIFICATION OF UNDERWATER ELECTROSTATIC FIELD INTENSITY DISTRIBUTION CHARACTERISTICS

To verify the correctness of the theoretical derivation and simulation results, as shown in Fig. 11(a), a glass tank with a size of $130.0 \times 60.0 \times 78.0$ cm is used to simulate the three-layer rectangular marine

environment in the laboratory. The sea water depth $D = 38.0$ cm, and the measured conductivity of sea water is 0.716 S/m at the temperature of 24.4° . The platinum sheet electrodes with parallel surfaces, 1.0×1.0 cm in size and 2.0 cm in spacing, are arranged along the x direction, and the center is located at $(x_0, y_0, z_0) = (0.0, 0.0, 10.0)$ cm. A constant current $I = 0.05$ A is applied in the direction of Fig. 11(a) to simulate the electric dipole field source. On $z = 19.0$ cm plane, nine solid Ag/AgCl electrodes of the same size are used to form a detection array along the y direction, and the distance between the two adjacent electrodes is 5.0 cm.

Limited by the experimental conditions, in order to obtain the E_x and E_y distributions on the depth plane, the above-mentioned linear array is scanned along the x direction to measure scalar potential, and the measured results are removed from the range and background noise. Then, as shown in Figs. 11(b), (c), the average gradient in the x and y directions of adjacent measured scalar potential field points is taken as the field strength measurement at the midpoint. The values are:

$$E_x(x, y, z) = \frac{\Phi\left(x + \Delta x/2, y, z\right) - \Phi\left(x - \Delta x/2, y, z\right)}{\Delta x} \quad (17)$$

$$E_y(x, y, z) = \frac{\Phi\left(x, y + \Delta y/2, z\right) - \Phi\left(x, y - \Delta y/2, z\right)}{\Delta y} \quad (18)$$

The measured results are shown in Figs. 12(a), (b). Using the aforementioned field source and ocean environment parameters, E_x and E_y on the plane $z = 19.0$ cm are calculated by Equations (12) and (13). The results are shown in Figs. 12(c), (d). Figs. 12(e), (f), and (g) show the theoretical values of E_x and E_y on three fields, $y = 15.0$ and $z = 19.0$ cm, $x = -52.5$ and $z = 19.0$ cm, $y = 15.0$ and $z = 19.0$ cm, respectively. The measured results are compared with the theoretical values of E_x and E_y in the case of no-shore bank model and shore-bank model.

From the graph, E_x and E_y are in good agreement with the theoretical simulation results under the condition with bank. By comparing with the condition of no bank, the former one can better describe the distribution characteristics of underwater electrostatic field of warships in the corresponding marine environment.

5. CONCLUSIONS

In this paper, the distribution characteristics of underwater electric fields of ships in four typical restricted seas are studied by theoretical derivation, numerical simulation, and experimental verification. The study draws the following conclusions. (1) In the above typical restricted waters, the general characteristics of underwater electrostatic intensity distribution of warship are consistent with those without shore walls, and still have obvious passing characteristics. (2) In the normal direction of the bank, the effects of vertical and parallel banks on the three-component field intensity are more obvious when the site is closer to the shore wall. In the tangent direction of the bank, the shore wall influences E_x more when the site is closer to the section which crosses the ship's field source and perpendicular to the bank. For E_y , the site located in the section is not influenced by boundary. When the vertical distance between the field point and the above section increases, E_y increases first and then decreases. The influence of the bank wall on E_z is related to the orientation of the bank wall. The rule of the vertical bank wall is consistent with E_x , while that of the parallel bank wall is consistent with E_y . (3) Under the same conditions, the effect of vertical bank on underwater electric field is greater than that of parallel bank. (4) For three layers of right-angle, archipelagos, and rectangular sea area, the field model can be regarded as a combination of three layers of vertical and parallel bank models. The law of the influence of bank boundary on field intensity distribution is the superposition of the influence of a single bank.

The conclusion of this paper is significant for using electric field signals to improve the accuracy of detection, identification, and strike of electromagnetic fuze, buoy, and array in restricted waters such as straits, archipelagic waterways, and port berths. In addition, the field models established in this paper can simulate the complex marine environment and the boundary of laboratory containers through the combination of different azimuths and numbers of shore banks, so it has a wide range of applicability.

ACKNOWLEDGMENT

This work is supported by the National Natural Science Foundation of China (Grant No. 51109215).

REFERENCES

1. Hu, S., B. Yan, and Y. Wang, "Ship tracking with static electric field based on adaptive progressive update extended Kalman filter," *MATEC Web of Conferences*, 232, 2018.
2. Chung, H. J., C. S. R. X. Yang, and J. J. Jeon, "A study on analysis method of underwater electric field signature due to ship's corrosion and corrosion protection system," *Journal of the Korea Institute of Military Science and Technology*, Vol. 11, No. 2, 1017–1021, 2008.
3. Solberg, J. R., K. M. Lynch, and M. A. Maciver, *Active Electrolocation for Underwater Target Localization*, Sage Publicatin, Inc., 2008.
4. Miller, R. C., "Active shaft grounding and diagnostic system," U.S. Patent, Oct. 10, 1989.
5. Wang, X. J., Q. L. Xu, J. C. Zhang, et al., "Simulating underwater electric field signal of ship using the boundary element method," *Progress In Electromagnetics Research M*, Vol. 76, 43–54, 2018.
6. Montoya, R., O. Rendon, and J. Genesca, "Mathematical simulation of a cathodic protection system by finite element method," *Materials and Corrosion*, Vol. 56, No. 6, 404–411, 2005.
7. Bian, Q., D. H. Liu, and X. J. Wang, "Research on underwater static electric field for warship based on hybrid model," *Applied Mechanics and Materials*, Vol. 713–715, 925–929, 2015.
8. Chen, C., D. G. Li, and S. G. Gong, "Research on the static magnetic field related with corrosion and anticorrosion of ship based on the electric dipole model," *Acta Armamentarll*, Vol. 31, No. 1, 113–118, 2010.
9. Morel, Y., V. Lebastard, and F. Boyer, "Neural-based underwater surface localization through electrolocation," *2016 International Conference on Robotics and Automation (ICRA)*, 2596–2603, IEEE, May 2016.
10. Du, L., S. C. Liu, J. J. Li, et al., "Experimental study on monitoring water flow and transport in sands by 2-D electrical resistivity tomography method," *EJGE*, Vol. 19, 10533–10537, 2014.